Solar Energy 196 (2020) 168–176

Contents lists available at ScienceDirect

Solar Energy

journal homepage: www.elsevier.com/locate/solener

Efficient inverted organic solar cells with a thin natural biomaterial L-Arginine as electron transport layer

Jianfeng Li[a,*], Ningning Wang[a], Yufei Wang[a], Zezhou Liang[a], Yichun Peng[c], Chunyan Yang[a], Xichang Bao[b,*], Yangjun Xia[a]

[a] School of Materials Science and Engineering, Lanzhou Jiaotong University, Lanzhou 730070, China
[b] Qingdao Institute of Bioenergy and Bioprocess Technology, Chinese Academy of Sciences, Qingdao 266101, China
[c] School of Civil Engineering, Lanzhou Institute of Technology, Lanzhou, Gansu 730050, China

ARTICLE INFO

Keywords:
Organic solar cells
L-Arginine
Electron transfer layer
Interfacial dipoles
Stability

ABSTRACT

Proper interfacial modification is a necessary condition for high-performance organic solar cells (OSCs). In this work, L-Arginine (L-Arg) with the advantages of low price, friendly environment and widespread existence in natural was successfully introduced into inverted OSCs as electron transport layer (ETL). Compared to the devices without ETL (bare ITO), the open circuit voltage (V_{OC}), short circuit current density (J_{SC}) and power conversion efficiency (PCE) of the ITO/L-Arg /PTB7-Th:$PC_{71}BM$/MoO_3/Ag device was increased to 0.77 V, 17.25 mA cm^{-2} and 9.00% from 0.36 V, 14.99 mA cm^{-2}, 1.90%, respectively. What's more, the photovoltaic performance of the device with ZnO/L-Arg double ETL was further improved (PCE (9.31%)). The excellent PCE resulting from the improved work function and the increased interface conductivity, and thus more effective carrier extraction and collection. Furthermore, the lifetime of the device with ZnO/L-Arg double ETL was significantly increased in comparison with that of with pure ZnO ETL. The results indicated that double ETL formed by the introduction of L-Arg, which provides an efficient, low-cost, green and healthy method for the preparation of high-performance OSCs.

1. Introduction

The unique advantages of mechanical flexibility, light weight, low cost and environmental friendliness make organic solar cells (OSCs) widely available (Bao et al.,2017; Chen et al., 2019a; Du et al., 2018; Kang et al., 2019; Wang et al., 2019a; Gao et al., 2019; Liu et al., 2016). After development for the decades, the power conversion efficiency (PCE) of OSCs have been increased to over 15% in single-junction binary devices (Fan et al., 2019; Yuan et al., 2019). However, the problem of bad stability and relatively low efficiency make it unable to meet the requirements of commercial applications. The synthesis of stable and excellent photoactive layer materials, optimization of device structure and interface engineering are important strategy to improve stability and efficiency. Among of these, interfacial engineering is an efficient approach to obtain relatively high PCE and stability. The interfacial layer is responsible for optimizing carrier transport, improving interface barrier, balancing propagation and distribution of light, affecting surface affinity of electrode and optimizing morphology of active layer (He et al., 2011; Huang et al., 2016; Kang et al., 2012; Zhang et al., 2014; Zheng et al., 2018). Hence, interfacial layer plays a vital role in OSCs, and needs to further explore new interfacial materials for improving interface and device performance (Kang et al., 2018; Liu et al., 2016; Rasool et al., 2019; Savva and Choulis, 2013; Wang et al., 2019c; Wei et al., 2017). Inorganic metal oxides, such as Cs_2CO_3, TiOx and ZnO (Yang et al., 2010; Steim et al., 2008) and alcohol/water-soluble conjugated polymer (He et al., 2012; Huang et al., 2004) and the small molecule electrolyte (Jia et al., 2016; Osikowicz et al., 2004) were widely used as electron transport layer (ETL). Among them, the ZnO film with the advantages high transparency, good conductivity, low cost and simple solution-processed is the most widely used as inorganic ETLs (Steim et al., 2008; Osikowicz et al., 2004). However, sometimes ZnO degraded device performance (Znaidi, 2010) mainly due to its non-self-healing defects as recombination centers in the surface under low annealing temperature. While high-quality ZnO film was commonly obtained at higher annealing temperatures, it is detrimental to the simple preparation of OSCs. Therefore, small molecular electrolytes with functional polar groups are contemplated to be the most effective ETL, owing to formation of dipoles at the interface, improved work function (WF) of ITO and reduction of interface barrier (Kim et al., 2007; Wang et al., 2019c). Furthermore, most small molecular

* Corresponding authors.
E-mail addresses: ljfpyc@163.com (J. Li), baoxc@qibebt.ac.cn (X. Bao).

https://doi.org/10.1016/j.solener.2019.11.101
Received 14 August 2019; Received in revised form 11 November 2019; Accepted 29 November 2019
Available online 13 December 2019

interfaces have self-assembly properties on ITO or metal oxides, and the ordered monolayer assembled film is formed by covalent bond on solid surface, which is defined as self-assembled monolayers (SAMs) (Pujari et al., 2014). SAMs exist a bi-directional adjustable effect on the WF of ITO substrate (Campbell et al., 1996; Zhou et al., 2012), mainly because the polar functional groups contained therein acting as interfacial modifiers, which maintain adhesion to ITO facilitates the preparation of active layer (Liu et al., 2003). The compounds of phosphoric acid, carboxylic acid, silane and amino group are commonly used as SAMs to modify ITO, however, most of them use toxic solvents in the process of preparation and treatment. Biological small molecules are the most potential substitutes for the development of interfacial materials because of their green and environment-friendly characteristics. Amino acids in the natural biomaterials have the inherent advantages of low cost, friendly environment and widespread existence. More importantly, they have good hydrophilic carboxy groups and are soluble in water solution. At the same time, they contain polar amino groups, which are easy to form strong hydrogen bonds with metal oxides and adsorb on the surface of metal oxides. Consequently, amino acids can be deposited uniformly on the ITO electrode by simple methods such as ink jet, rotating coating and so on (Liu et al., 2003; Deng, et al., 2014; Li et al., 2014). Moreover, the existence of polar amino group may result in the formation of interface dipole moment and reduced WF of ITO, which is possible to improve the PCE of OSCs. However, amino acids are widely found in nature as biological materials, have not been paid enough attention to in OSC.

In this work, L-Arginine (L-Arg), non-toxic and water soluble biomaterial, as ETL was successfully introduced into inverted OSCs based on PTB7-Th:$PC_{71}BM$. The results show that the PCE of ZnO/L-Arg double ETL OSCs is 9.31%, which is higher than that of L-Arg (9.00%) and pure ZnO (8.09%). This is mainly due to the fact that L-Arg significantly reduces the WF of ITO, makes the modified ITO have a good energy level matching with acceptor material ($PC_{71}BM$) in active layer, and realizes highly efficient and stable inverted OSCs. The WF and interaction of ITO modified by different ETLs were analyzed by ultraviolet electron spectroscopy (UPS) and X-ray photoelectron spectroscopy (XPS). The improved conductivity of the device was proved by space charge-limited current (SCLC), impedance spectrum (IS) and *J-V* under dark condition. Moreover, the interfaces were characterized by atomic force microscope (AFM) and water contact angle (WCA). These results showed that, after inserting L-Arg interface, the improvement of photovoltaic performance in OSCs was due to the formation of dipole moment at the interface, the decreased WF of ITO, the improved charge extraction ability and enhanced electron transport ability.

2. Experimental section

2.1. Materials

ITO with a sheet resistance of 15 Ω square^{-1} was acquired from CSG Holding Co. Ltd. PTB7-Th was purchased from Calos. $PC_{71}BM$ and chlorobenzene (CB) were bought from Sigma-Aldrich. MoO_3 (99.99%) and Ag (99.99%) were obtained from Alfa (Zhengzhou, China). L-Arginine (99.00%) was purchased from Aladdin. ZnO was produced using the method of the reported literature (Borse et al., 2018). 3,3′-(1,3,8,10-Tetraoxoanthra[2,1,9-def:6,5,10-d'e'f']diisoquinoline-2,9(1*H*,3*H*,8*H*,10*H*)-diyl)bis(*N*,*N*-dimethylpropan-1-amine oxide) (PDINO) was bought from Derthon optoelectronic materials science technology Co LTD.

2.2. Device fabrication

The utilized inverted device structure with ITO/ZnO (L-Arg or ZnO/ L-Arg)/PTB7-Th:$PC_{71}BM$/MoO_3/Ag and the corresponding materials were shown in. Fig. 1. The prepared methods of ITO glass substrates, active layer, MoO_3 and Ag were consistent with previous work (Li et al., 2018, 2019). However, the only difference was employing 3% diphenyl sulfide (DPS) as additive in active layer. The ZnO solution was spin-coated onto the ITO substrates at 3500 rpm for 40 s and then thermal annealed at 120 ℃ for 10 min in air to form ITO/ZnO film. The L-Arg dissolved in deionized water at a concentration of 0.5–4 mg/mL and was spun onto the ITO or ITO/ZnO at 2500 rpm for 40 s for different thickness devices (the concentration is 0.5 mg/mL, 1 mg/mL, 2 mg/mL and 4 mg/mL corresponding to the L-Arg thickness of 4 nm, 6 nm, 8 nm, and 13 nm). The film thickness was determined according to the method (Wu et al., 2004). It is worth noting that the L-Arg solution is heated at 40 ℃ for an hour before spinning. The area of the OSCs is 0.10 cm^2.

2.3. Device characterization

The test conditions and methods were similar to our previous work with *J-V* curves, EQE, WCA, IS, AFM and film thickness (Wang et al., 2019d). The transmission spectra of the four films were recorded by UV-1800 spectrophotometer (Shimadzu Company). The UPS/XPS was measured on AXIS ULTRA DLD (Kratos, Japan).

3. Results and discussion

Fig. 2 shows the transmittance spectra of ZnO, L-Arg and ZnO/L-Arg films on ITO substrate. For comparison, we have also measured the transmittance of bare ITO substrate. The anti-reflection effect of ZnO increased transmittance (Wu et al., 2015; Gupta et al., 2013), which was reflected in transmit spectrum of ITO/ZnO and ITO/ZnO/L-Arg in the range of 360–440 nm. For the wavelength ranging from 450 to 600 nm, the transmittance shapes of ITO/ZnO/L-Arg and ITO/L-Arg are quite similar, which demonstrated the high transmittance of L-Arg. Thus, we could infer that L-Arg has tiny effect on light loss of active layer.

To explore the influence of L-Arg on ITO and ZnO, their surfaces were analyzed by XPS. The full XPS spectra were shown in Fig. 3(a), and Gaussian functions to fit the peak position of N and O. In Fig. 3(b), the characteristic peaks N (1s) of L-Arg was observed, indicating that L-Arg had been successfully deposited on the surface of ZnO and ITO. The high resolution XPS spectra of N (1s) for ITO/L-Arg and ZnO/L-Arg films exhibited two asymmetric peaks at 400.95 eV and 399.47 eV, the former peak can be attributed to the nitrogen atoms in the neutral amines and the latter one could be ascribed to one of protonated amines. (Song et al., 2013; Deng et al., 2014; Li et al., 2014). The positive charge amines (protonated amines) of the cationic of L-Arg interact strongly with the negative charge terminal oxygen ions of the ITO or ZnO surface (Kang et al., 2012). In Fig. 3(c), the O (1s) spectra of the ZnO film can be split into two peaks at 531.26 eV, contributed by Zn⊖O bonding, 532.68 eV corresponded to hydroxyl group (Yan et al., 2017). Compared to the O (1s) peak of ZnO, the O (1s) peak of ZnO/L-Arg decreased by 0.26 eV from 532.68 eV to 532.42 eV, therefore, the core level shift toward the lower binding suggested that the existed electrostatic interaction led to a higher negative charge density of O atoms (Tengstedt et al., 2006), which was due to the formation of strong dipoles between L-Arg and ITO or ZnO interfaces. Therefore, the surface dipole moment pointing outwards from ITO can reduce WF of ITO through a downward vacuum level shift, so that the ITO/L-Arg or ITO/ZnO/L-Arg electrode can be used as the low WF cathode of inverted OSCs. Meanwhile, the strong interface interaction is helpful to suppress the interface energy barrier and improve the contact between the electrode and the active layer (Tan et al., 2018).

To investigate the development of different interface layers on ITO WF, we measured the electronic properties of ZnO, L-Arg and ZnO/L-Arg on ITO substrates by UPS as shown in Fig. 4. The value of WF was determined from the cut-off edge of kinetic energy according to the method discussed in the literature (Sun et al., 2012). It can be clearly seen that the WF of pure ITO is − 4.71 eV. The addition of L-Arg

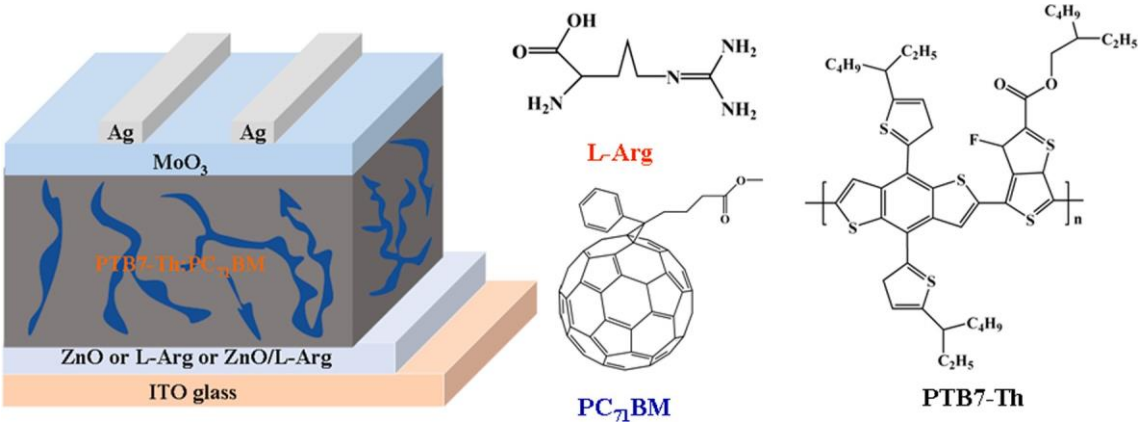

Fig. 1. The schematic diagram of OSCs and chemical structure with L-Arg, PTB7-Th and $PC_{71}BM$.

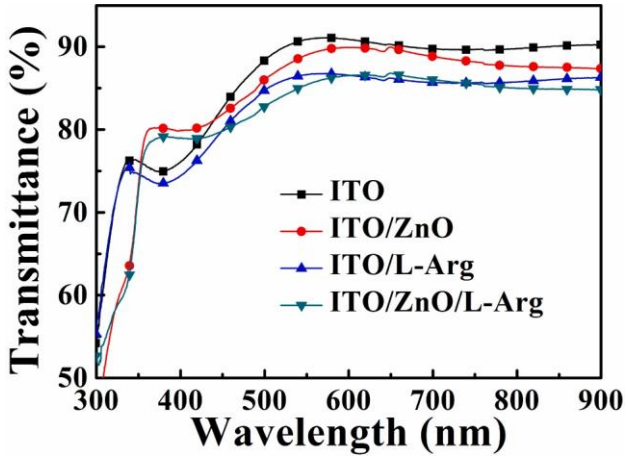

Fig. 2. Optical transmittance spectra gained from different ETLs.

(−3.97 eV) made the WF of ITO substrate lower than that of pure ZnO (−4.34 eV) due to interface dipoles interaction formed by amino acid on the surface of ITO processed by self-assembly. Compared with the pure L-Arg interface, the WF of ZnO/L-Arg (−3.74 eV) double interface ran lower than the pure L-Arg interface. It has been prooed that the reduction WF of the ITO/ZnO/L-Arg interface could improve the electronic selectivity and build-in potential of organic devices (Kang et al., 2012; Mihailetchi et al., 2003; Schlaf et al., 1998). Furthermore, the WF of ZnO/L-Arg becomes closer to the lowest unoccupied molecular orbital (LUMO) energy level of $PC_{71}BM$ (−4.00 eV), which would reduce electron charge extraction barrier from interface layer to the cathode and improve ohmic contact and built-in field. The photovoltaic devices with ZnO/L-Arg interface layer could have higher V_{OC} and FF than ZnO layer.

To further explore the ascendancy of the L-Arg interface layer on device performance, inverted OSCs with L-Arg ETL were fabricated. The current density-voltage (*J-V*) curves of the OSCs with different concentrations of L-Arg are given in Fig. S1 and Table S1, and the optimized device with J_{SC} of 17.25 mA cm^{-2}, FF of 67.80% and PCE of 9.00% was obtained when the concentration is 2 mg mL^{-1}. Moreover, L-Arg film was easily aggregated when increasing concentrations, which can affect charge collection and result in poor device performance. Thus, the aqueous solution of L-Arg must be strictly required within a low concentration range. Fig. 5(a) shows the *J-V* curves of OSCs with four different conditions (ITO, ITO/ZnO, ITO/L-Arg, and ITO/ZnO/L-Arg films). The V_{OC}, J_{SC} and *FF* of the device without ETL are 0.36 V, 14.99 mA cm^{-2}, 35.76%, respectively, which leads to a lower PCE of

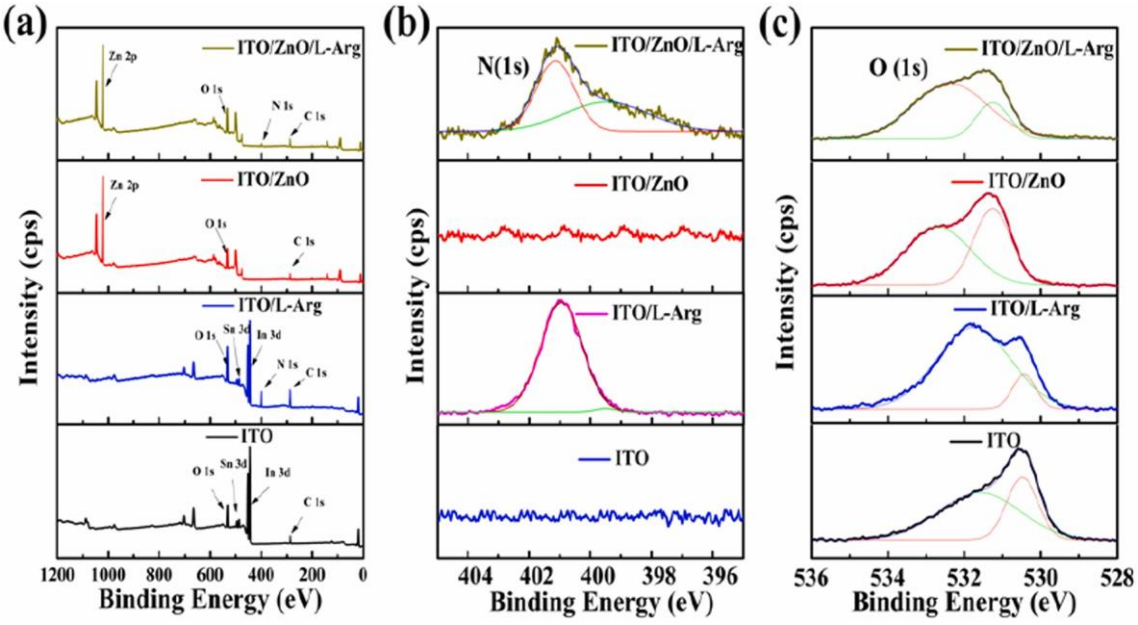

Fig. 3. (a) Survey X-ray photoelectron spectra. (b) N 1s and (c) O 1s XPS spectra obtained from different ETLs.

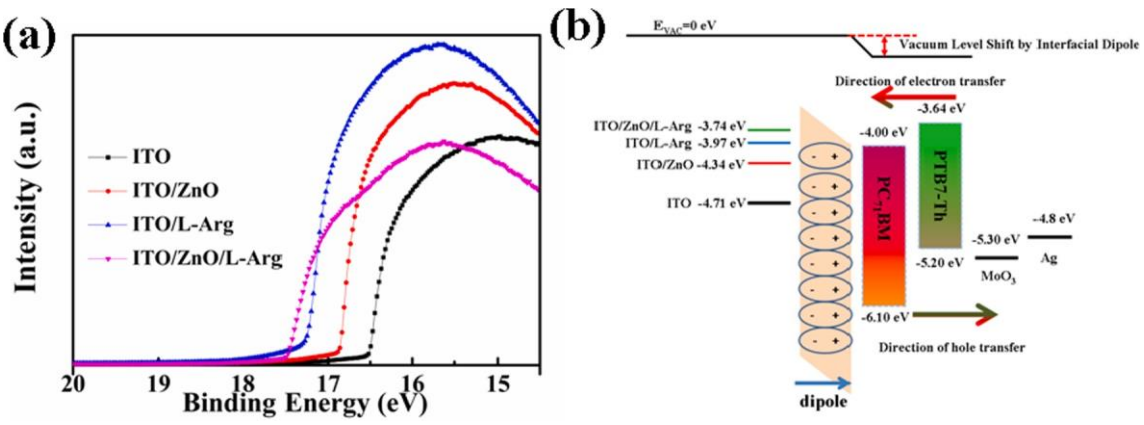

Fig. 4. (a) The UPS spectra of the different ETLs. (b) Energy level diagram of the OSCs with different ETLs.

1.90%. When ZnO was used as ETL, the PCE is markedly increased to 8.09%. When L-Arg is used as ETL, the PCE of the device is slightly improved to 9.00% which mainly benefited from further enhanced J_{SC} of 17.25 mA cm^{-2} and *FF* of 67.80%. The best performance was obtained from the device with L-Arg modified ZnO interface layer, and the value of V_{OC}, J_{SC}, FF and PCE are 0.78 V, 17.49 mA cm^{-2}, 68.22%, and 9.31%, respectively. In addition, the device with ITO/ZnO/L-Arg has the minimum R_s (3.71 $\Omega \cdot cm^2$) and the maximum R_{sh} (1166.86 $\Omega \cdot cm^2$), which could lead to the decrease of charge recombination rate and increase of charge extraction rate. For further comparison, external quantum efficiency (EQE) curves of the devices with four different conditions are shown in Fig. 5(b). All devices exhibit high quantum efficiency in the wavelength range of 300 to 750 nm. The device with ITO/ZnO/L-Arg film presents the maximum EQE of 80%, which is higher than the device with ZnO film (74%). The J_{SC} obtained by integrating the EQE data is consistent with the results from *J-V* curves as given in Table 1. The EQE responses of ETL with L-Arg and ZnO/L-Arg double interface device are better than that of bare ITO and with ZnO ETL. The EQE spectra ameliorated by L-Arg are consistent with the increasing trend of J_{SC}, indicating that it has strong charge collection ability.

To investigate the effect of introducing L-Arg interface layer on device performance, we characterized the exciton dissociation of different devices. J_{ph} is photocurrent density, J_L is current density under illumination and J_D is dark conditions. V_{eff} is determined by the equation of V_{eff} $V_{\_}$ V_{appl}, where V_{eff} is effective bias voltage, V_{appl} is the applied voltage and V_0 is the voltage at $J_D = J_L$ (Gao et al., 2019; Wang et al., 2019b). Fig. 6 shows J_{ph} increased with V_{eff} in the low range for both devices and saturated at a high V_{eff}, suggesting that the photogenerated excitons are dissociated into free charge carriers and collected at the electrodes (Zhou et al., 2016). The device with ZnO/L-Arg double interlayer has the highest J_{ph} and reaches saturation faster than the devices with ZnO and L-Arg interface layer. It means that devices could harvest more efficient exciton dissociation and carrier collection with the double interface. According to the equation G_{max} J_{sat}/qL (q is the electronic charge and L (100 nm) is the thickness of active layer) (Shrotriya et al., 2006), the J_{sat} is correlated to the maximum exciton generation rate G_{max}, which is mainly governed by the light absorption. The G_{max} values of the OSCs are 1.08 $\times$ 10^{28}, 1.10 $\times$ 10^{28}, and 1.15 $\times$ 10^{28}, 1.17 $\times$ 10^{28} m^{-3} s^{-1}, corresponding to the device without interface layer and with ZnO, L-Arg and ZnO/L-Arg, respectively. The detailed G_{max} values of OSCs are given in Table 2. When L-Arg was used as the interface layer, it made for the increasing of photogenerated carriers, especially when the ZnO/L-Arg was used as the double interface, which is propitious to the production of a lot of excitons dissociation and charges collection in OSCs. For OSCs, not all excitons could be dissociated into free carriers. Therefore, J_{ph}/J_{sat} is defined as the exciton dissociation rate P (E, T). In the case of short circuit current, the P (E, T) values of the devices with the pure ITO and other three kinds of different interfaces are 34.75%, 92.60%, 93.27%, and 93.17%, respectively. It is clear that the interface of L-Arg is advantageous to the dissociation of exciton. At the same time, the exciton dissociation performance of the device with ZnO/L-Arg double interface layer gets superior to the other two devices with single interface layer. Interestingly, the difference among the P (E, T) values of the three devices was not obvious, so the enhancement of J_{SC} and FF could be due to other reasons.

To further investigate the effect of the introduction of L-Arg on charge transfer performance of the devices, the electron-only devices with different ETLs were fabricated and tested, whose structure is ITO/ZnO (or L-Arg or ZnO/L-Arg)/active layer/PDINO/Al. Eq. (1) shows the relationship of SCLC, which is derived from Mott-Gurney's law (Liang

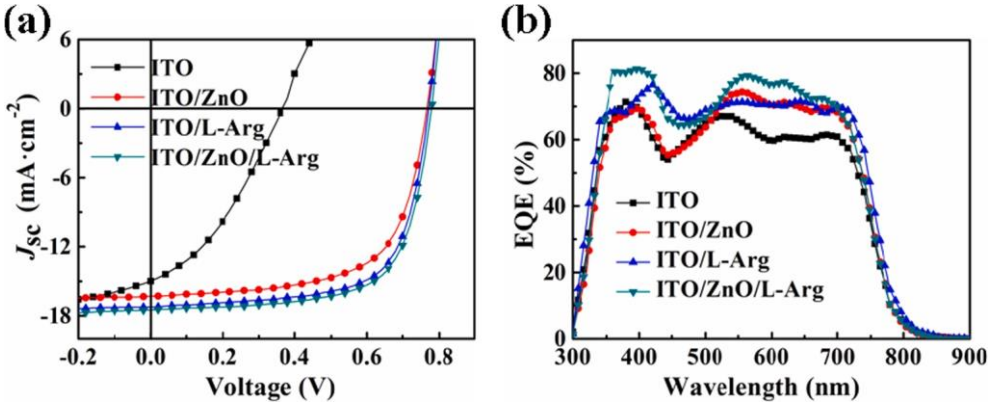

Fig. 5. (a) The *J-V* and (b) the EQE curves of different ETLs devices.

Table 1
Performance data of different interface layer photovoltaic devices.

ETL	V_{OC} (V)	J_{SC}[a] (mA cm^{-2})	FF (%)	PCE[b] (%)	R_s (Ω·cm^2)	R_{sh} (Ω·cm^2)
ITO	0.36 ± 0.003	14.99 ± 0.44 (14.74 ± 0.64)	35.76 ± 0.53	1.90 ± 0.26	15.62	76.11
ITO/ZnO	0.77 ± 0.003	16.30 ± 0.33 (16.06 ± 0.56)	64.45 ± 0.52	8.09 ± 0.25	4.52	854.88
ITO/L-Arg	0.77 ± 0.002	17.25 ± 0.24 (17.02 ± 0.37)	67.80 ± 0.41	9.00 ± 0.21	3.92	1042.75
ITO/ZnO/L-Arg	0.78 ± 0.002	17.49 ± 0.34 (17.21 ± 0.52)	68.22 ± 0.47	9.31 ± 0.25	3.71	1166.86

[a] The values in parentheses is from EQE calculation.
[b] The statistical results were obtained from 5 independent cells, and the ± refer to the standard deviation.

et al., 2019; Chen et al., 2019b).

$$J = \frac{9}{8}\varepsilon_0\varepsilon_r \mu \frac{(V_{appl} - V_{bi})^2}{L^3} \quad (1)$$

J is the current density, ε_0 is the permittivity of free space (8.85×10^{-12}F/m), ε_r is the dielectric constant of the bulk heterojunction (BHJ) layer (≈3.00), μ is the hole mobility, d is the active layer thickness (100 nm), V_{appl} is the applied voltage, and V_{bi} is the built-in voltage produced from the difference in the WF of the cathode and the anode, μ is mobility. V_{appl}-V_{bi} is the voltage drop across device. For the Hole-only devices, V_{bi} is 0 V, while V_{bi} is 0.7 V in the electron-only devices. The prepared condition of the active layers here are the duplicate for the preceding devices. The *J-V* curves for SCLC was measured under dark condition, as shown in Fig. 7. Electron mobility increased from 1.89×10^{-4} cm^2 V^{-1} s^{-1} (ZnO), 2.36×10^{-4} cm^2 V^{-1} s^{-1} (L-Arg), and finally up to 3.61×10^{-4} cm^2 V^{-1} s^{-1} (ZnO/L-Arg), and the results are consistent with the trend of PCE. It could be seen that electron transport ability of L-Arg interface increased than that of ZnO interface and the electron transport ability of ZnO/L-Arg interface was higher than that of pure L-Arg interface, implying the device with ZnO/L-Arg double interlayer achieves the largest electron current density. The analysis of SCLC showed that the ZnO/L-Arg led to the enhancement of electron mobility, indicating the good arrangement of energy levels and the effectiveness of the extraction with electrons from the active layer, which is explained for the better J_{SC} and FF in the double interface device structure system.

To better monitor the electron transport ability of different interface layers, devices with structure of ITO/ETL/Ag were fabricated. Fig. 8(a) shows the dark *J-V* characteristics of three different ETL devices, and all exhibit ohmic behavior (Wang et al., 2016). The conductivity of the L-Arg layer was higher than that of the ZnO layer, indicating that the electron transport ability gets more effective in the device with L-Arg interface layer and the related series resistance becomes much smaller. Compared with ZnO, L-Arg, the device with ZnO/L-Arg double interface has further decreased series resistance, which is beneficial to restrain the charge recombination of OSCs and promote the extraction of electrons. This may be due to the L-Arg penetration filled the ZnO interface defect in the double interface layer, it prevented the ZnO from recombination into larger and non-conductive particles (Mbule et al., 2013). This is consistent with the results obtained by the atomic force microscope discussed below.

Table 2
G_{max} and corresponding J_{ph}/J_{sat} values of the OSCs with different ETLs.

ETLs	*P (E, T)*	G_{max} (m^{-3} s^{-1})
ITO	34.75%	1.08×10^{28}
ZnO	92.60%	1.10×10^{28}
L-Arg	93.27%	1.15×10^{28}
ZnO/L-Arg	93.17%	1.17×10^{28}

To analyze the influence of interface materials on charge recombination, the devices of ITO, ZnO, L-Arg and ZnO/L-Arg were analyzed by means of impedance spectroscopy (IS), as shown in Fig. 8(b). The composite resistance of the device can be obtained by the impedance spectrum of the Nyquist diagram. The impedance spectra of the devices show a semicircle shape, and the diameter of the reduced semicircle in the diagram represents the impedance values of three different interface devices (ZnO, L-Arg and ZnO/L-Arg). Small diameter represents a smaller impedance value, which has been proved to be beneficial to electron transport (Choi et al., 2011). The results show that the introduction of L-Arg layer reduced the diameter of the impedance semicircle, which indicates the decreased of the impedance value of the device. Interestingly, the impedance diagram of the ZnO/L-Arg double interface device got the smallest diameter, so its impedance value was the smallest, which may be due to the good film-forming property of the ZnO/L-Arg interface and increased coalescent with the active layer and thus decreased the interface resistance (Guo et al., 2019), which was consistent with the results of interfacial morphology.

The dark current curve of the device could reflect the changes of the series resistance (R_s) and the parallel resistance (R_{sh}) of the device, which has important reference for evaluating the performance of OSCs. The dark state curve of the OSCs can be divided into three regions (Waldauf et al., 2006): in the negative voltage region, there is a

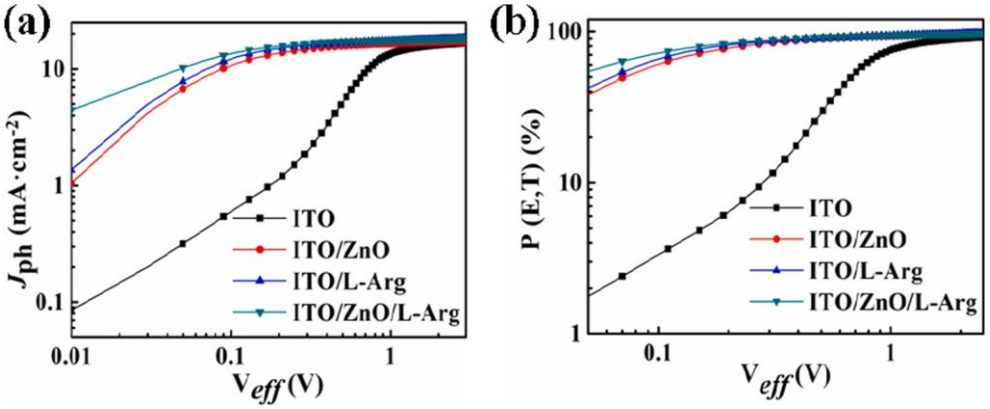

Fig. 6. The four different interfaces curves of (a) Photocurrent density (J_{ph}) and effective voltage (V_{eff}) curves as well as (b) exciton dissociation probability P (E, T) values and effective voltage (V_{eff}).

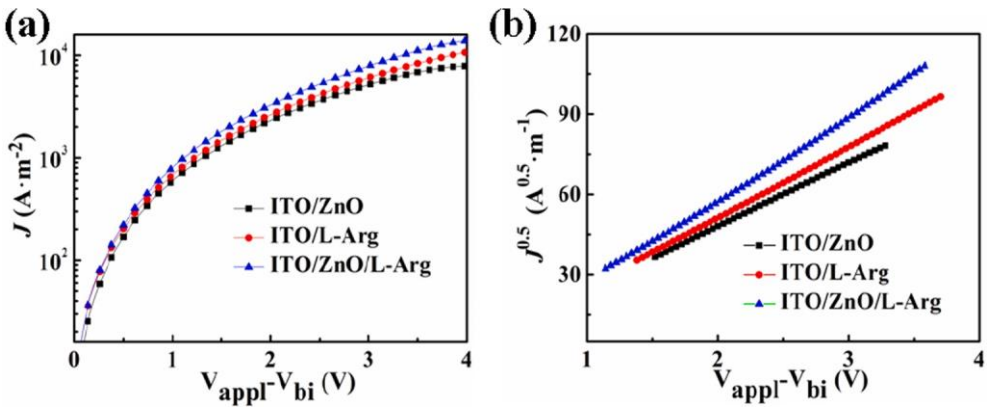

Fig. 7. (a) *J–V* and (b) $J^{0.5}$–*V* characteristic curves of electron-only devices with three species of ETLs.

symmetrical small current that flows through the cell leakage current, which determined by the R_{sh} in the cells. At relatively low voltage, the positive current increases exponentially, indicating that the device has the rectifier characteristics of diode. With further increases voltage, the current growth rate decreases due to the tunneling effect and the limitation of space charge transfer (Potscavage et al., 2009). Therefore, the current is determined by R_s in the device, which got linearly relate to voltage. As shown in Fig. 9. In the range of −2 to 2 V, the reverse and leakage current of the L-Arg or ZnO/L-Arg interlayer are significantly lower than the bare ITO device. It is reported that one of the reasons for the increasing of V_{OC} gets the reduction of reverse dark current (He et al., 2010), in which case, in the range of −2 to 0 V, the reverse dark current density of the device with L-Arg or ZnO/L-Arg ETL was greatly reduced, and compared with the device on bare ITO, the V_{OC} was greatly increased from 0.36 to 0.78 V. In the 0–2 V range, the starting voltage of the L-Arg or ZnO/L-Arg interlayer remains 0.7–0.8 V and the transport layer free device is only 0.3–0.4 V, indicating that when L-Arg or ZnO/L-Arg ETL was used, the built-in potential (V_{bi}) of the devices increased. The calculated value of R_s, R_{sh} listed in Table 1. The R_S values of L-Arg and ZnO/L-Arg devices were 3.92 and 3.71 Ω·cm^2, respectively, which was lower than the control device based on bare ITO (15.62 Ω·cm^2) and ZnO (4.52 Ω·cm^2). This provided an explanation for the increasing of J_{SC} from 14.99 and 16.30 to 17.25 or 17.49 mA cm^{-2}. In addition, the R_{sh} values of the devices based on bare ITO, ZnO, L-Arg and ZnO/L-Arg are 76.11, 854.88, 1042.75 and 1166.86 Ω·cm^2, respectively, indicating that OSCs fabricated by L-Arg or ZnO/L-Arg interlayer exist a lower leakage current trend and exhibit stronger diode characteristics. This goes in good agreement with the decreasing of leakage current and the increasing of V_{OC}. As a result, the performance of devices for ZnO/L-Arg or L-Arg as the ETL could be improved because good OSCs required high R_{sh} and low R_s. These effects improved *FF* from 35.76% (pure ITO) and 64.45% (ZnO devices) to 67.80% (L-Arg devices) and 68.22% (ZnO/L-Arg), respectively.

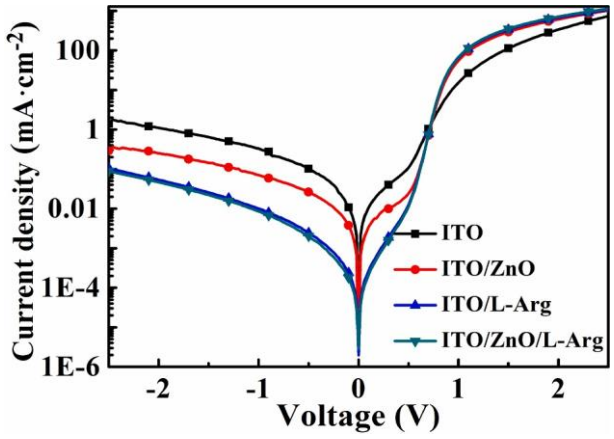

Fig. 9. *J–V* characteristic curves of OSCs with different ETLs in the dark.

To further study the relationship between the vertical component distribution of PTB7-Th:$PC_{71}BM$ and ETLs, the surface energies of the active layer (PTB7-Th and $PC_{71}BM$) and different ETLs were measured by contact angle measurements. The contact angle data and the corresponding surface energy calculated by Owens method were listed in Table S2. The rich degree of acceptor on the substrate can be qualitatively measured based on the enthalpy value (ΔG) between the donor or acceptor and the substrate interface. ΔG can be obtained by Good's Eq. (2):

$$\Delta G \quad -2(\sqrt{r_1^d \; r^d{}_2} \quad \sqrt{r_1^p \quad r_2^p}) \tag{2}$$

here the subscripts 1 and 2 are the PTB7-Th or $PC_{71}BM$ and the

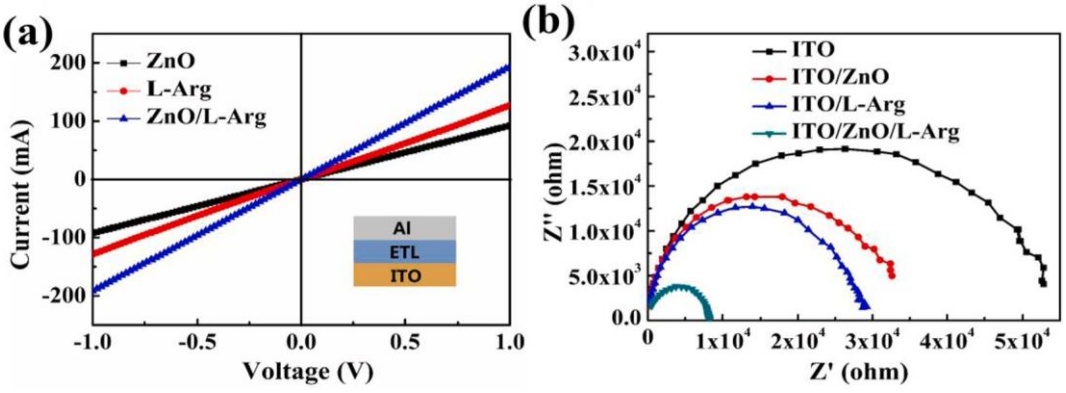

Fig. 8. *J–V* curves of devices in the dark and device structure diagram for electrical conductivity measurement and (b) Nyquist plot of the OSCs with different ETL.

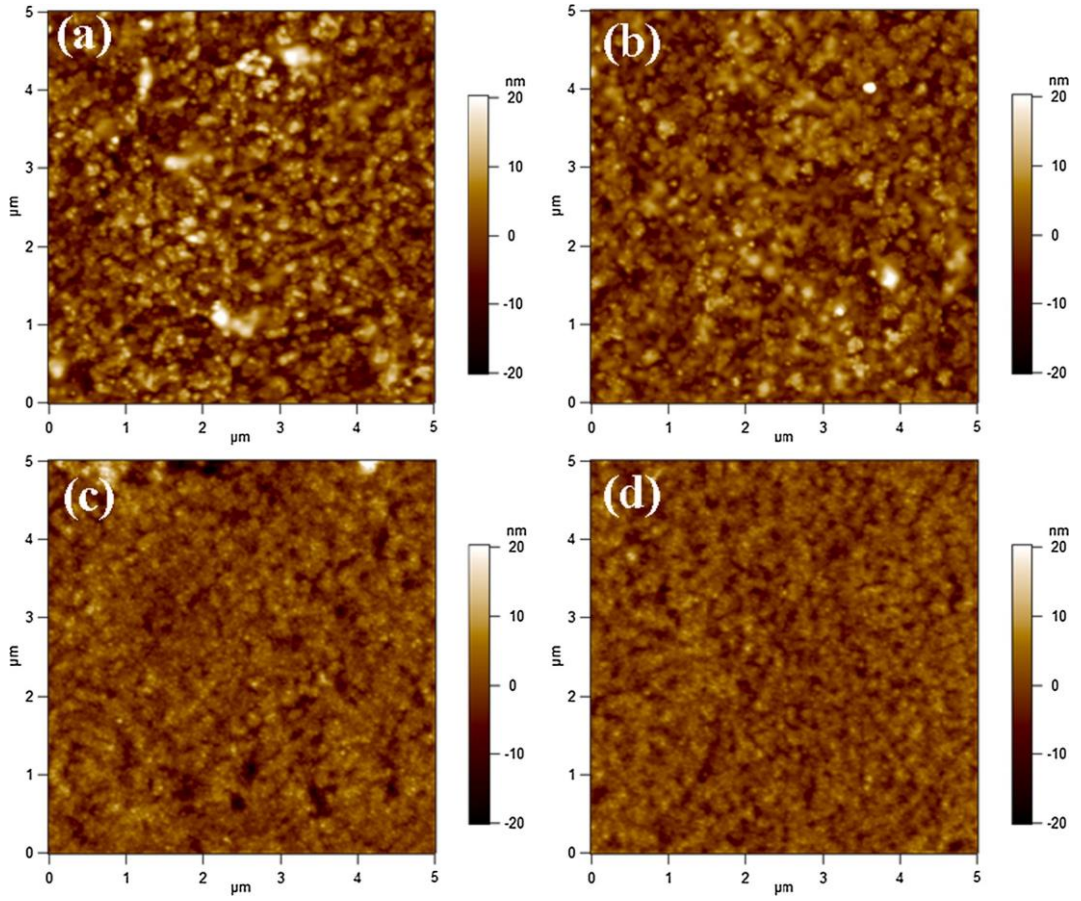

Fig. 10. The 2D (a–d) topographic AFM images of different ETLs.

substrate, respectively. Superscripts d and p represent the non-polar and polar component of the surface energy. The calculated results are shown in Table S3. The more negative ΔG value between the two materials, the more stable interface can be formed. The relative degree of acceptor-rich (Δ) on the substrate is related to the enthalpy ratio of donor /acceptor substrate. When Δ value is greater than 1, there is an acceptor-enriched layer. The Δ values of the active layer materials on four different substrates are all greater than 1 (Table S4). Notably, the Δ value on ZnO/L-Arg was the largest, indicating that more $PC_{71}BM$ might be distributed at the bottom of photoactive layers, which will facilitate the transmission and collection of electrons and improve the performance of the OSCs (Fan et al., 2011).

To investigate the development of amino acids on the morphology of modified ITO, the ETLs on ITO substrate were determined by AFM. The AFM height-images (a-d) are shown in Fig. 10. The root-mean-square (RMS) roughness values of bare ITO, ITO/ZnO, ITO/L-Arg, and ITO/ZnO/L-Arg are 5.32 nm, 4.54 nm, 3.65 nm and 3.08 nm, respectively, indicating that the modification of amino acid has a certain effect on surface morphology. The roughness of ZnO surface was larger than L-Arg surface, and the distribution got not uniform and anomalistic bumps and pinholes were caught on the modified ITO, which could be caused by reunited of ZnO nanoparticles (Huang et al., 2018). Compared with ZnO thin films, the surface of ITO/ZnO/L-Arg films was quite smooth with the RMS value decreased to 0.89 nm, indicating that L-Arg could pad the gaps and pinholes of ZnO film and make the surface smooth. Therefore, it was proposed that L-Arg film could fill defects of the ZnO nanoparticles. The results clearly exhibit that the reduction of the roughness of ZnO film could improve the corresponding device performance, which is consistent with the previous report (Ouyang et al., 2016). The change of surface roughness could be seen from 3D (Fig. 10 (e ~ f)) diagram. The uniform smooth surface of the ITO/ZnO/L-Arg interlayer facilitates better contact on the active layer, which depressed the probability of interfacial charge recombination and heightened the amount of electron extraction, leading to an increase of device efficiency. This result has the analogic trend with the dark *J-V* characteristics of the device.

In addition to the PCE, the stability of the device is more and more important to the OSCs. Since the OSCs with ZnO/L-Arg dual interfaces have the highest PCE, we preliminarily investigated the stability of double ETL devices in nitrogen filled glove box, together with the referenced devices with pure ZnO ETL, the result is shown in Fig. 11. After 35 days, the average PCE of OSCs with ZnO/L-Arg double ETL was

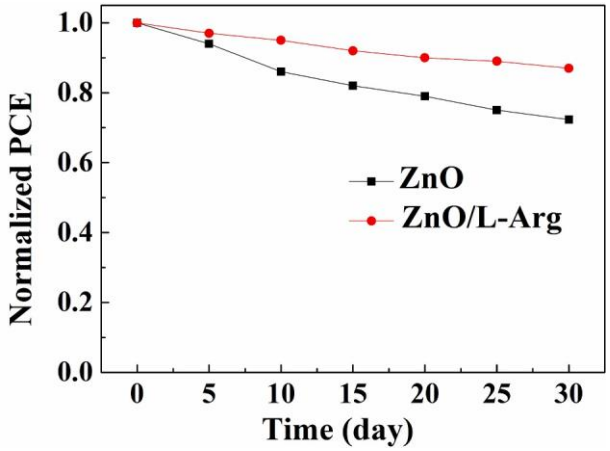

Fig. 11. PCEs of the OSCs with ZnO and ZnO/L-Arg ETL respectively as a function of storage time.

maintained about 87%, while that of OSCs with pure ZnO ETL was maintained about 72% of the original value. The decrease of OSCs with pure ZnO ETL is mainly due to the non-uniform and defects containing surface of the ZnO ETL (Ling et al., 2019; Polydorou, et al., 2017; Musselman et al., 2014). Modification of the ETL with the L-Arg is one way to mitigate these native surface defects of ZnO and thereby enhancing the efficient flow of electrons across the junction.

4. Conclusion

In this work, amino acid L-Arg was used on the ITO or ZnO to form an interface modification layer for OSCs. Compared with pure ZnO, inverted device based on PTB7-Th:$PC_{71}BM$ as active layer, and L-Arg as cathode interfacial layer, J_{SC} was increased from 16.30 mA cm^{-2} to 17.49 mA cm^{-2} and the PCE was increased from 8.09% to 9.31%. According to the results of XPS, UPS, SCLC, IS, conductivity, *J-V* under dark condition, WCA and AFM, we found that the application of ZnO/L-Arg reduces the WF of ITO and improves vertical phase segregation, which reduces interface barrier and improves charge extraction and collection, as well as suppresses exciton recombination, and thus decreases leakage current of related devices. In addition, the surface morphology of the ITO/ZnO/L-Arg interface is more uniformity and smooth, which is beneficial to contact between the interface and the active layer, resulting in improving the efficiency of OSCs. Furthermore, the lifetime of the device with ZnO/L-Arg double ETL significantly increased in comparison with that of device with pure ZnO ETL in a nitrogen-filled glove box without encapsulation. The results show that L-Arg of natural biomaterials can be used to prepare the ETL of OSC, which provides a new way to fabricate the ETL of OSCs with low cost, non-toxic and environmentally friendly.

Acknowledgements

The authors thank the National Natural Science Foundation of China (no. 61964010; 51602139), the Natural Science Foundation of Gansu Province (no. 18JR3RA108), Excellent Team of Scientific Research (201705), the Foundation of A Hundred Youth Talents Training and Instrument Analysis Center of Lanzhou Jiaotong University.

Appendix A. Supplementary material

Supplementary data to this article can be found online at https://doi.org/10.1016/j.solener.2019.11.101.

References

Bao, X., Zhang, Y., Wang, J., Zhu, D., Yang, C., Li, Y., Yang, C., Xu, J., Yang, R., 2017. High extinction coefficient thieno[3,4-b]thiophene-based copolymer for efficient fullerene-free solar cells with large current density. Chem. Mater. 29, 6766–6771.

Borse, K., Sharma, R., Gupta, D., Yella, A., 2018. Interface engineering through electron transport layer modification for high efficiency organic solar cells. RSC Adv. 8, 5984–5991.

Campbell, I.H., Rubin, S., Zawodzinski, T.A., Kress, J.D., Martin, R.L., Smith, D.L., Barashkov, N.N., Ferraris, J.P., 1996. Controlling Schottky energy barriers in organic electronic devices using self-assembled monolayers. Phys. Rev. B. 54, 14321–14324.

Chen, W., Huang, G., Li, X., Li, Y., Wang, H., Jiang, H., Zhao, Z., Yu, D., Wang, E., Yang, R., 2019a. Revealing the position effect of an alkylthio side chain in phenyl-substituted benzodithiophene-based donor polymers on the photovoltaic performance of non-fullerene organic solar cells. ACS Appl. Mater. Interfaces. 11, 33173–33178.

Chen, W., Shen, W., Wang, H., Liu, F., Duan, L., Xu, X., Zhu, D., Qiu, M., Wang, E., Yang, R., 2019b. Enhanced efficiency of polymer solar cells by improving molecular aggregation and broadening the absorption spectra. Dyes Pigments 166, 42–48.

Choi, H., Park, J.S., Jeong, E., Kim, G.H., Lee, B.R., Kim, S.O., Song, M.H., Woo, H.Y., Kim, J.Y., 2011. Combination of titanium oxide and a conjugated polyelectrolyte for high-performance inverted-type organic optoelectronic devices. Adv. Mater. 232759–232763.

Deng, X., Nie, R., Li, A., Wei, H., Zheng, S., Huang, W., Mo, Y., Su, Y., Wang, Q., Li, Y., Tang, J., Xu, J., Wong, K., 2014. Ultra-low work function transparent electrodes achieved by naturally occurring biomaterials for organic optoelectronic devices. Adv. Mater. Interfaces 1, 1400215.

Du, Z., Bao, X., Li, Y., Liu, D., Wang, J., Yang, C., Wimmer, R., Stade, L.W., Yang, R., Yu, D., 2018. Balancing high open circuit voltage over 1.0 V and high short circuit current in benzodithiophene-based polymer solar cells with low energy loss: a synergistic effect of fluorination and alkylthiolation. Adv. Energy Mater. 8, 1701471.

Fan, B., Zhang, D., Li, M., Zhong, W., Zeng, Z., Ying, L., Huang, F., Cao, Y., 2019. Achieving over 16% efficiency for single-junction organic solar cells. China Chem. 62, 1–7.

Fan, X., Fang, G., Guo, S., Liu, N., Gao, H., Qin, P., Li, S., Long, H., Zheng, Q., Zhao, X., 2011. Controllable synthesis of flake-like Al-doped ZnO nanostructures and its application in inverted organic solar cells. Nano Res. Lett. 6, 546.

Gao, K., Jo, S.B., Shi, X., Nian, L., Zhang, M., Kan, Y., Lin, F., Kan, B., Xu, B., Rong, Q., Shui, L., Liu, F., Peng, X., Zhou, G., Cao, Y., Jen, A., 2019. Over 12% effciency nonfullerene all-small-molecule organic solar cells with sequentially evolved multi-length scale morphologies. Adv. Mater. 31, 1807842.

Guo, J., Ren, G., Han, W., Sun, Y., Wang, M., Zhou, Y., Shen, L., Guo, W., 2019. Facilitating electron extraction of inverted polymer solar cells by using organic/inorganic/organic composite buffer layer. Org. Electron. 68, 187–192.

Gupta, S.K., Sharma, A., Banerjee, S., Gahlot, R., Aggarwal, N., Deepak, Garg, A., 2013. Understanding the role of thickness and morphology of the constituent layers on the performance of inverted organic solar cells. Sol. Energy Mater. Sol. Cells. 116, 135–143.

He, Z., Zhong, C., Wu, H., Yang, R., Yang, W., Huang, F., Bazan, G.C., Cao, Y., 2010. Origin of the enhanced open-circuit voltage in polymer solar cells *via* interfacial modification using conjugated polyelectrolytes. J. Mater. Chem. 20, 2617–2622.

He, Z., Zhong, C., Huang, X., Wong, W., Wu, H., Chen, L., Su, J., Cao, Y., 2011. Simultaneous enhancement of open-circuit voltage, short-circuit current density, and fill factor in polymer solar cells. Adv. Mater. 23, 4636–4643.

He, Z., Zhong, C., Su, S., Xu, M., Wu, H., Cao, Y., 2012. Enhanced power-conversion efficiency in polymer solar cells using an inverted device structure. Nat. Photonics 6, 591–595.

Huang, F., Wu, H., Wang, D., Yang, W., Cao, Y., 2004. Novel electroluminescent conjugated polyelectrolytes based on polyfluorene. Chem. Mater. 16, 708–716.

Huang, L., Chen, L., Huang, P., Wu, F., Tan, L., Xiao, S., Zhong, W., Sun, L., Chen, Y., 2016. Triple dipole effect from self-assembled small-molecules for high performance organic photovoltaics. Adv. Mater. 28, 4852–4860.

Huang, Y., Chen, H., Lin, H., We, K., 2018. Doping ZnO electron transport layers with MoS_2 nanosheets enhances the efficiency of polymer solar cells. ACS Appl. Mater. Interfaces 10,20196–20204.

Jia, X., Wu, N., Wei, J., Zhang, L., Luo, Q., Bao, Z., Li, Y., Yang, Y., Liu, X., Ma, C., 2016. A low-cost and low-temperature processable zinc oxide-polyethylenimine (ZnO:PEI) nano-composite as cathode buffer layer for organic and perovskite solar cells. Org. Electron. 38, 150–157.

Kang, H., Hong, S., Lee, J., Lee, K., 2012. Electrostatically self-assembled nonconjugated polyelectrolytes as an ideal interfacial layer for inverted polymer solar cells. Adv. Mater. 24, 3005–3009.

Kang, Q., Yang, B., Xu, Y., Xu, B., Hou, J., 2018. Printable MoOx anode interlayers for organic solar cells. Adv. Mater. 30, 1801718.

Kang, Q., Ye, L., Xu, B., An, C., Stuard, S.J., Zhang, S., Yao, H., Ade, H., Hou, J., 2019. A printable organic cathode interlayer enables over 13% efficiency for 1 cm^2 organic solar cells. Joule 3, 227–239.

Kim, J.S., Park, J.H., Lee, J.H., Jo, J., Kim, D.Y., Cho, K., 2007. Control of the electrode work function and active layer morphology via surface modification of indium tin oxide for high efficiency organic photovoltaics. Appl. Phys. Lett. 91, 112111.

Li, A., Nie, R., Deng, X., Wei, H., Zheng, S., Li, Y., Tang, J., Wong, K., 2014. Highly efficient inverted organic solar cells using amino acid modified indium tin oxide as cathode. Appl. Phys. Lett. 104, 123303.

Li, J., Liang, Z., Wang, Y., Li, H., Tong, J., Bao, X., Xia, Y., 2018. Enhanced efficiency of polymer solar cells through synergistic optimization of mobility and tuning donor alloys by adding high-mobility conjugated polymers. J. Mater. Chem. C. 6, 11015–11022.

Li, J., Wang, Y., Liang, Z., Wang, N., Tong, J., Yang, C., Bao, X., Xia, Y., 2019. Enhanced organic photovoltaic performance through modulating vertical composition distribution and promoting crystallinity of the photoactive layer by diphenyl sulfide additives. ACS Appl. Mater. Interfaces 11, 7022–7029.

Liang, Z., Tong, J., Li, H., Wang, Y., Wang, N., Li, J., Yang, C., Xia, Y., 2019. The comprehensive utilization of the synergistic effect of fullerene and non-fullerene acceptors to achieve highly efficient polymer solar cells. J. Mater. Chem. A.7, 15841–15850.

Liu, C., Zhang, L., Xiao, L., Peng, X., Cao, Y., 2016. Doping ZnO with water/alcohol-soluble small molecules as electron transport layers for inverted polymer solar cells. ACS Appl Mater. Interfaces 8, 28225–29230.

Liu, X., Mohamed, S.H., Ngaruiya, J.M., Wuttig, M., Michely, T., 2003. Modifying the growth of organic thin films by a self-assembled monolayer. Appl. Phys. 93, 4852–4855.

Mbule, P.S., Kim, T.H., Kim, B.S., Swart, H.C., Ntwaeaborwa, O.M., 2013. Effects of particle morphology of ZnO buffer layer on the performance of organic solar cell devices. Sol. Energy Mater. Sol. Cells. 112, 6–12.

Mihailetchi, V.D., Blom, P.W.M., Hummelen, J.C., Rispens, M.T., 2003. Cathode dependence of the open-circuit voltage of polymer:fullerene bulk heterojunction solar cells. J. Appl. Phys. 94, 6849–6854.

Musselman, K.P., Albert-Seifried, S., Hoye, R.L.Z., Sadhanala, A., Munoz-Rojas, D., Macmanus-Driscoll, J.L., Friend, R.H., 2014. Improved exciton dissociation at semiconducting polymer: ZnO donor: acceptor interfaces via nitrogen doping of ZnO. Adv. Funct. Mater. 24, 3562–3570.

Osikowicz, W., Crispin, X., Tengstedt, C., Lindell, L., Kugler, T., Salaneck, W.R., 2004. Transparent low-work-function indium tin oxide electrode obtainedby molecular

scale interface engineering. Appl. Phys. Lett. 85, 1616–1618.
Ouyang, X., Peng, R., Ai, L., Zhang, X., Ge, Z., 2016. Efficient polymer solar cells employing a non-conjugated small-molecule electrolyte. Nat. Photonics 9, 520–524.
Polydorou, E., Sakellis, I., Soultati, A., Kaltzoglou, A., Papadopoulos, T.A., Briscoe, J., Tsikritzis, D., Fakis, M., Palilis, L.C., Kennou, S., Argitis, P., Falaras, P., Davazoglou, D., Vasilopoulou, M., 2017. Avoiding ambient air and light induced degradation in high-efficiency polymer solar cells by the use of hydrogen-doped zinc oxide as electron extraction material. Nano Energy 34, 500–514.
Potscavage, W.J., Sharma, J.A., Kippelen, B., 2009. Critical interfaces in organic solar cells and their influence on the open-circuit voltage. ACC Chem. Res. 42, 1758–1767.
Pujari, S.P., Scheres, L., Marcelis, A.T.M., Zuilhof, H., 2014. Covalent surface modification of oxide surfaces. Chem. Int. Ed. 53, 6322–6356.
Rasool, Shafket, Doana, Vu., Lee, H.K., Lee, S.K., Lee, J.C., Moon, S.J., So, W.W., Song, C.E., Shin, W.S., 2019. Enhanced photostability in polymer solar cells achieved with modified electron transport layer. Thin Solid Films 669, 42–48.
Savva, A., Choulis, S.A., 2013. Cesium-doped zinc oxide as electron selective contact in inverted organic photovoltaics. Appl. Phys. Lett. 102, 23301.
Schlaf, R., Parkinson, B.A., Lee, P.A., Nebesny, K.W., Jabbour, G., Kippelen, B., Peyghambarian, N., Armstrong, N.R., 1998. Photoemission spectroscopy of LiF coated Al and Pt electrodes. Appl. Phys. 84, 6729–6736.
Shrotriya, V., Yao, Y., Li, G., Yang, Y., 2006. Effect of self organization in polymer/fullerene bulk heterojunctions on solar cell performance. Appl. Phys. Lett. 89, 063505.
Song, M., Kang, J., Kim, D.H., Kwon, J.D., Park, S.G., Nam, S., Jo, S., Ryu, S.Y., Kim, C.S., 2013. Self-assembled monolayer as an interfacial modification material for highly efficient and air-stable inverted organic solar cells. Appl. Phys. Lett. 102, 143303.
Steim, R., Choulis, S.A., Schilinsky, P., Brabec, C.J., 2008. Interface modification for highly efficient organic photovoltaics. Appl. Phys. Lett. 92, 093303.
Sun, K., Zhao, B., Kumar, A., Zeng, K., Ouyang, J., 2012. Highly efficient, inverted polymer solar cells with indium tin oxide modified with solution-processed zwitterions as the transparent cathode. ACS Appl. Mater. Interfaces 4, 2009–2017.
Tan, Y., Chen, L., Wu, F., Huang, B., Liao, Z., Yu, Z., Hu, L., Zhou, Y., Chen, Y., 2018. Regulation of the polar groups in n-type conjugated polyelectrolytes as electron transfer layer for inverted polymer solar cells. Macromolecules 51, 8197–8204.
Tengstedt, C., Osikowicz, W., Salaneck, W.R., Parker, I.D., Hsu, C.H., Fahlman, M., 2006. Fahlman, Fermi-level pinning at conjugated polymer interfaces. Appl. Phys. Lett. 88, 053502(1)-(4).
Waldauf, C., Scharber, M.C., Schilinsky, P., Hauch, J.A., Brabec, C.J., 2006. Physics of organic bulk heterojunction devices for photovoltaic applications. J. Appl. Phys. 99, 104503.
Wang, J., Yan, C., Zhang, X., Zhao, X., Fu, Y., Zhang, B., Xie, Z., 2016. High-efficiency polymer solar cells employing solution-processible and thickness-independent gallium-doped zinc oxide nanoparticles as cathode buffer layers. J. Mater. Chem. C. 4, 10820–10826.
Wang, X., Du, Z., Dou, K., Jiang, H., Gao, C., Han, L., Yang, R., 2019a. A maverick asymmetrical backbone with distinct flanked twist angles modulating the molecular aggregation and crystallinity for high performance nonfullerene solar cells. Adv. Energy Mater. 9, 1802530.
Wang, X., Dou, K., Shahid, B., Liu, Z., Li, Y., Sun, M., Zheng, N., Bao, X., Yang, R., 2019b. Terpolymer strategy toward high-efficiency polymer solar cells: integrating symmetric benzodithiophene and asymmetrical thieno[2,3-f]benzofuran segments. Chem. Mater. 31,6163–6173.
Wang, Y., Liang, Z., Li, X., Qin, J., Ren, M., Yang, C., Bao, X., Xia, Y., Li, J., 2019c. Self-doping n-type polymer as cathode interface layer enables efficient organic solar cells by increasing built-in electric field and boosting interface contact. J. Mater. Chem. C. 7, 11152–11159.
Wang, Y., Liang, Z., Qin, J., Tong, J., Guo, P., Cao, X., Li, J., Xia, J., 2019d. An alcohol-soluble polymer electron transport layer based on perylene diimide derivatives for polymer solar cells. IEEE J. Photovolt. 9, 1678–1685.
Wei, J., Yin, Z., Chen, S., Zheng, Q., 2017. Low-temperature solution-processed zinc tin oxide film as a cathode interlayer for organic solar cells. ACS Appl. Mater. Interfaces 9, 6186–6193.
Wu, H., Huang, F., Mo, Y., Yang, W., Wang, D., Peng, J., Cao, Y., 2004. Efficient elecreon injection from a bilayer cathode consisting of aluminum and alcohol-/water-soluble conjugated polymers. Adv. Mater. 16, 1826–1830.
Wu, N., Luo, Q., Bao, Z., Lin, J., Li, Y., Ma, C., 2015. Zinc oxide: conjugated polymer nanocomposite as cathode buffer layer for solution processed inverted organic solar cells. Sol. Energy Mater. Sol. Cells 141, 248–259.
Yang, T., Cai, W., Qin, D., Wang, E., Lan, L., Gong, X., Peng, J., Cao, Y., 2010. Solution-processed zinc oxide thin film as a buffer layer for polymer solar cells with an inverted device structure. Phys. Chem. C. 114, 6849–6853.
Yan, Y., Cai, F., Yang, L., Li, J., Zhang, Y., Qin, F., Xiong, C., Zhou, Y., Lidzey, D.G., Wang, T., 2017. Light-soaking-free inverted polymer solar cells with an effciency of 10.5% by compositional and surface modifcations to a low-temperature-processed TiO_2 electron-transport layer. Adv. Mater. 29, 1604044.
Yuan, J., Zhang, Y., Zhou, L., Zhang, G., Yip, H.L., Lau, T.K., Lu, X., Zhu, C., Peng, H., Johnson, P.A., Leclerc, M., Cao, Y., Ulanski, J., Li, Y., Zou, Y., 2019. Single-junction organic solar cell with over 15% efficiency using fused-ring acceptor with electron-deficient core. Joule 3, 1140–1151.
Zhang, Z., Qi, B., Jin,Z., Chi,D., Qi,Z., Li, Y., Wang, J., 2014. Perylene diimides: a thickness-insensitive cathode interlayer for high performance polymer solar cells, Energy Environ. Sci. 7, 1966–1973.
Zhou, M., Sun, Q., Gao, L., Wu, J., Zhou, S., Li, Z., Hao, Y., Shi, F., 2016. Enhancement of power conversion efficiency of PTB7:PCBM-based solar cells by gate bias. Org. Electron. 32, 34–40.
Zhou, Y., Fuentes-Hernandez, C., Shim, J., Meyer, J., Giordano, A.J., Li, H., Winget, P., Papadopoulos, T., Cheun, H., Kim, J., Fenoll, M., Dindar, A., Haske, W., Najafabadi, E., Khan, T.M., Sojoudi, H., Barlow, S., Graham, S., Brédas, J.L., Marder, S.R., Kahn, A., Kippelen, B., 2012. A universal method to produce low-work function electrodes for organic electronics. Science 336, 327–332.
Zheng, Z., Hu, Q., Zhang, S., Zhang, D., Wang, J., Xie, S., Wang, R., Qin, Y., Li, W., Hong, L., Liang, N., Liu, F., Zhang, Y., Wei, Z., Tang, Z., Russell, T., Hou, J., Zhou, H., 2018. A highly efficient non-fullerene organic solar cell with a fill factor over 0.80 enabled by a fine-tuned hole-transporting layer. Adv. Mater. 30, 1801801.
Znaidi, L., 2010. Sol–gel-deposited ZnO thin films: a review. Mater. Sci. Eng. B. 174, 18–30.

Further reading

Gao, K., Zhu, Z., Xu, B., Jo, S.B., Kan, Y., Peng, X., Jen, A.K.Y., 2017. Highly efficient porphyrin-based OPV/perovskite hybrid solar cells with extended photoresponse and high fill factor. Adv. Mater. 29, 1703980.